Properties of $R\mathrm{Re}_2\mathrm{Al}_{10}$ (R=Y, Gd–Lu) crystals

Athena S. Sefat, Sergey L. Bud'ko, and Paul C. Canfield
Department of Physics and Astronomy, Ames Laboratory, Iowa State University, Ames, Iowa 50011, USA
(Received 17 March 2009; published 22 May 2009)

Large single crystals of rare-earth rhenium aluminide $R\mathrm{Re}_2\mathrm{Al}_{10}$, with R=Y, and Gd–Lu were grown out of an Al-rich solution. Single crystal x-ray diffraction data confirmed the orthorhombic *Cmcm* structure for all members: R=Gd-Dy with $\mathrm{TbRe}_2\mathrm{Al}_{10}$-structure type (formula unit per cell Z=8); R=Y, and Ho–Lu with $\mathrm{LuRe}_2\mathrm{Al}_{10}$-structure type ($Z$=12). There is no evidence of a localized 3*d* electron moment in R=Y and Lu; R=Yb is nonmagnetic down to 1.8 K, but develops an enhanced electronic specific heat of ~95 mJ mol^{-1} K^{-2}. Ordering temperatures range from ferromagnetic order in R=Gd with T_c=7.2(1) K, antiferromagnetic order in R=Tb at T_N=5.0(3) K, to R=Dy, Ho, and Er giving magnetic ordering temperatures of T_{mag}=1.7(1), ≤0.4, and 1.1(2) K, respectively. All compounds have effective moments close in value to that of free R^{3+} at high temperatures.

DOI: 10.1103/PhysRevB.79.174429 PACS number(s): 75.50.−y

I. INTRODUCTION

In the past few decades, ternary rare-earth (R) transition-metal (T) aluminide systems of $R\mathrm{T}_4\mathrm{Al}_8$, $R\mathrm{T}_6\mathrm{Al}_6$ (T=Cr, Mn, Fe, Co, Ni, Cu) (Refs. 1–7) and $R\mathrm{T}_2\mathrm{Al}_{10}$ (T=Mn) (Ref. 8) have attracted interest due to their diverse magnetic phenomena. Among such high aluminum content ternaries, the properties of rhenium based systems are unexplored. The rare-earth series of $R\mathrm{Re}_2\mathrm{Al}_{10}$ is the focus of this investigation.

In the $R\mathrm{Re}_2\mathrm{Al}_{10}$ structure, rare-earth atoms occupy two crystallographic sites, each having a coordination number of 20 (4 Re, 16 Al neighbors). The early rare-earths of R=Ce-Nd, and Sm adopt a tetragonal structure first reported for $\mathrm{CaCr}_2\mathrm{Al}_{10}$ ($P4/nmm$),[9,10] with 4 f.u. per cell (Z=4). The later rare-earths crystallize in orthorhombic structures: R=Gd and Tb in $\mathrm{TbRe}_2\mathrm{Al}_{10}$-structure type ($Cmcm$, Z=8),[11] and R=Ho-Lu in $\mathrm{LuRe}_2\mathrm{Al}_{10}$-structure type ($Cmcm$, Z=12).[12] The orthorhombic structures are characterized by two R positions with $m2m$, $2/m$ site symmetries in $\mathrm{TbRe}_2\mathrm{Al}_{10}$ and $m2m$, m in $\mathrm{LuRe}_2\mathrm{Al}_{10}$-structure types. In the $\mathrm{TbRe}_2\mathrm{Al}_{10}$ structure, the rhenium atoms occupy only one position with two Tb and ten Al neighbors in an icosahedral arrangement (CN=12). The aluminum atoms occupy nine unique crystallographic sites. Each Al has between 12 and 14 neighbors of which two are Re atoms, one or two are Tb atoms, and the rest are Al atoms. $\mathrm{TbRe}_2\mathrm{Al}_{10}$ structure consists of alternating rectangular close packed puckered Re:Al layer (A) and the less densely packed planer R:Al layer (B or B′). A total of eight layers are needed to complete one translation period in this structure (Fig. 1, left). Compared with this structure, $\mathrm{LuRe}_2\mathrm{Al}_{10}$ is essentially made from the same kind of layers, but 12 layers are needed to complete one stacking sequence in this structure (Fig. 1, right). In the $\mathrm{LuRe}_2\mathrm{Al}_{10}$, the two rhenium positions are in distorted icosahedral coordination

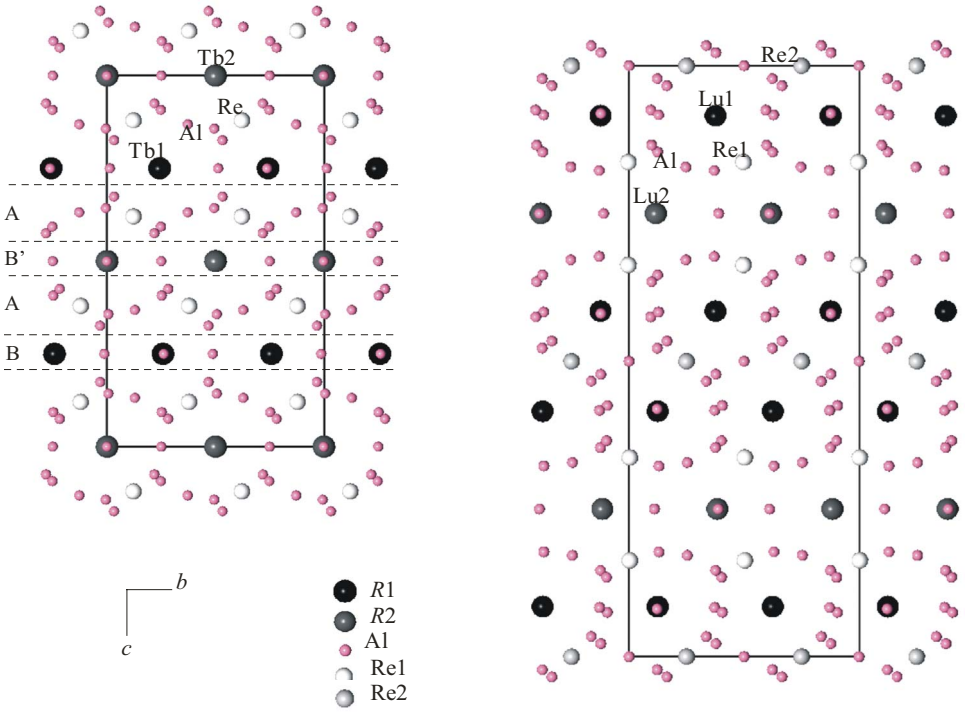

FIG. 1. (Color online) Structure types of $\mathrm{TbRe}_2\mathrm{Al}_{10}$ (left) and $\mathrm{LuRe}_2\mathrm{Al}_{10}$ (right). The layers are designated on the left side with the letters A, B, and B′.

of two Lu and ten Al atoms. The 12 different aluminum atoms have between 12 and 14 neighbors, of which two are Re and one or two are Lu atoms. For the first time, the R=Y and Dy members of $R\mathrm{Re}_2\mathrm{Al}_{10}$ are structurally identified and physical properties of the crystals with R=Y, and Gd–Lu members are investigated.

The substitution of rare earths accompanies changes in the magnetic properties throughout the $R\mathrm{Re}_2\mathrm{Al}_{10}$ series. The anisotropic field- and temperature-dependent magnetizations, as well as specific heat and resistivity data are compared. The experimental details below are followed by structural descriptions of these members. For each compound, the physical property results will presented and discussed.

II. EXPERIMENTAL DETAILS

The $R\mathrm{Re}_2\mathrm{Al}_{10}$ (R=Y, Gd–Lu) crystals were grown out of an Al-rich self-flux, similar to Ref. 8. For the preparation of these ternaries, high purity elements (>99.9%) of R:Re:Al in the atomic ratio of 4:8:88 were arc melted, placed in alumina crucibles, and sealed into fused silica tubes under $\sim\frac{1}{2}$ atmosphere argon. The crystals were synthesized by heating to 1200 °C, slow cooling (~5–6 °C/h) to 875 °C, and decanting off the flux by means of a centrifuge. The crystals formed as square prisms with shortest side parallel to the c-crystallographic axis. The typical dimensions of the single crystals were $\sim 3\times 5\times 5$ mm^3, however, the sizes and yields became smaller as the rare-earth ions became heavier. The batches with R=Yb and Lu produced the smallest crystals with dimensions generally less than $0.5\times 2\times 2$ mm^3.

Single crystal analyses were followed using STOE IPDS2 image plate x-ray diffractometer (Mo $K\alpha$ radiation).[13] Given that variations in stoichiometry may be a cause for discrepancy in magnetic order, a structural evaluation of the $R\mathrm{Re}_2\mathrm{Al}_{10}$ (R=Y, Gd–Lu) flux-grown crystals, with respect to lattice parameters and atomic site occupancies were done. The data were adjusted for Lorentz and polarization effects, and numerical absorption corrections were done using the X-SHAPE program.[14] The crystal structures were refined with the SHELXTL program suite.[15]

Magnetization was measured as a function of temperature, $M(T)$, and magnetic field, $M(H)$, using a Quantum Design magnetic property measurement system (MPMS). For a typical temperature sweep experiment, the sample was cooled to 1.8 K in zero-field (zfc) and data were collected by warming from 1.8 to 300 K in an applied field. The sample was then cooled in the applied field (fc), and the measurement repeated from 1.8 K. The notations $\|c$ (or $M_{\|c}$) denote magnetization measurements made with the applied field along the [001] crystallographic direction. The orthorhombic $R\mathrm{Re}_2\mathrm{Al}_{10}$ crystals have similar a- and b-lattice parameters and were not oriented within the plane. The magnetization measurements in the plane were done in two arbitrary directions, ~90° from each other ($\perp c1$ and $\perp c2$). Above the magnetic ordering, the $M(T)$ data were fitted to a modified Curie-Weiss law where $M/H\approx\chi=C/(T-\theta_\mathrm{p})+\chi_\mathrm{o}$, where χ is the magnetic susceptibility, C is the Curie constant, θ_p is the paramagnetic Curie-Weiss temperature, and χ_o is a temperature independent. In general the fits to the data were done above 50 K. If the rare earth is the only moment bearing ion, then the term C is related to the effective moment of the rare-earth ion in paramagnetic state and $\mu_\mathrm{eff}=g_J[J(J+1)]^{1/2}$, where J is the orbital moment. For Y^{3+} and Lu^{3+}, $\mu_\mathrm{eff}=0$. The polycrystalline average of the magnetization data may be estimated by $(M/H)_\mathrm{poly}\approx\chi_\mathrm{poly}=[\chi_{\|c}+\chi_{\perp c1}+\chi_{\perp c2}]/3$, where $\chi_{\perp c1}$ and $\chi_{\perp c2}$ are the two in-plane data sets as discussed above. For some compounds, the low-temperature data are presented in the form of $d(\chi T)/dT$,[16] to infer antiferromagnetic transition temperatures. For temperatures above magnetic ordering, the $M(T)$ data were fitted to modified Curie-Weiss law; this is done in an attempt to remove the effects of the crystalline electric field splitting, at least to the first order, from the effective moment and the paramagnetic temperature.[17,18]

Because the low-temperature ordered state of $\mathrm{GdRe}_2\mathrm{Al}_{10}$ has a ferromagnetic component, magnetization isotherms, in the vicinity of T_c, have been measured and used for the construction of an Arrott plot[19] in the form of M^2 versus $H_\mathrm{eff}M^{-1}$. H_eff estimates the effective field inside the sample and is found by subtracting the demagnetizing field H_d from the applied field ($H_\mathrm{d}=NM$, where N is the demagnetizing factor dependent on sample shape). For $\mathrm{GdRe}_2\mathrm{Al}_{10}$, demagnetization correction of 0.4 kOe/μ_B was used ($N\approx 0.1$ by approximating geometry as ellipse).

Temperature-dependent electrical resistivity measurements were also performed on the MPMS unit, interfaced with a LR 700 ac resistance bridge. A 16 Hz excitation current of 3 mA was applied. The electrical contacts were placed on samples in the standard four-probe geometry, using Pt wires and silver epoxy (EPO-TEK H20E). The current direction was in the ab plane for each sample. Residual-resistivity-ratios were found from the resistivity $\rho(T)$ data and defined as $\mathrm{RRR}=\rho(300\ \mathrm{K})/\rho(1.8\ \mathrm{K})$.

Specific heat, $C_\mathrm{p}(T)$ were measured using a Quantum Design PPMS, via the relaxation method. The R=Y, Gd, Tb, and Tm–Lu compounds were measured down to 1.8 K, and the data for R=Dy, Ho, and Er, were collected down to 0.4 K using a ^{3}He insert. Data were collected up to a maximum temperature of 50 K for Gd, 30 K for Tb and Dy, and 20 K for Ho. For the nonmagnetic compounds, a plot of C/T against T^2 gave a straight line with a slope β and intercept γ, associated with the lattice and electronic contributions, respectively. The value of the Debye temperature (θ_D) can be estimated in this low-temperature limit ($\beta=12\pi^4R/5\theta^3$). In order to obtain the magnetic specific heat for R=Gd-Dy members, nonmagnetic contributions (lattice and electronic effects) were approximated by the nonmagnetic $\mathrm{YRe}_2\mathrm{Al}_{10}$ data, and subtracted from their specific heat results. Since the unit cell parameters and molecular weight for Y sample is different from those of R=Gd-Dy, the C_p data of Y analog was scaled to Gd at 50 K, by multiplying 1.05. For R=Er member, the nonmagnetic contributions were approximated by $\mathrm{LuRe}_2\mathrm{Al}_{10}$, as they have similar lattice parameters and nearly the same mass (Table I). The magnetic entropy, S, was estimated by integration of C/T vs T after an extrapolation of the data down to the origin (i.e., for T=0 K, S=0) via polynomial fit. The fact that R ln 8 was recovered for $\mathrm{GdRe}_2\mathrm{Al}_{10}$

TABLE I. Single crystal and structure data for $R\mathrm{Re_2Al_{10}}$

	Y	Gd	Tb	Dy	Ho	Er	Tm	Yb	Lu
Z	12	8	8	8	12	12	12	12	12
a(Å)	9.3062(19)	9.3014(19)	9.2912(19)	9.2877(19)	9.2822(19)	9.2809(19)	9.2902(19)	9.3071(19)	9.2807(19)
b(Å)	10.308(2)	10.321(2)	10.310(2)	10.314(2)	10.298(2)	10.283(2)	10.278(2)	10.283(2)	10.255(2)
c(Å)	26.936(5)	18.048(4)	18.038(4)	18.011(4)	26.887(5)	26.860(5)	26.847(5)	26.857(5)	26.787(5)
V(Å^3)	2583.9(9)	1732.7(6)	1729.3(6)	1725.3(6)	2570.0(9)	2563.3(9)	2563.6(9)	2570.5(9)	2549.4(9)
$d_{\mathrm{calc.}}$ (Mg/m^3)	5.64	6.08	6.15	6.16	6.26	6.27	6.28	6.27	6.32
μ(Mo Kα)(mm^{-1})	35.7	36.0	36.9	37.3	38.1	38.9	39.3	39.6	40.9
Final R_1, $\mathrm{wR_2}[I>2\sigma(I)]^a$	0.0681, 0.1880	0.0362, 0.0880	0.0392, 0.1047	0.0288, 0.0649	0.0523, 0.1378	0.0465, 0.1188	0.0498, 0.1189	0.0553, 0.1580	0.0659 0.1762
Largest diff. Peak and hole (e Å^{-3})	4.33, −5.79	5.66, −7.33	6.91, −4.95	1.69, −1.70	4.51, −5.55	5.63, −11.03	5.78, −4.02	7.61 −4.69	9.96, −7.31

sample is taken as confirmation that the scaled $\mathrm{YRe_2Al_{10}}$ is an adequate approximation of the nonmagnetic excitations.

III. RESULTS AND DISCUSSION

A. Structure of $R\mathrm{Re_2Al_{10}}$ (R=Y, Gd–Lu)

The systematic absences and intensity statistics in all the data sets indicate that the structure of $R\mathrm{Re_2Al_{10}}$ (R=Y, Gd-Lu) is C centered, centrosymmetric, and orthorhombic (*Cmcm*, No. 63). The crystallographic structure of R =Gd-Dy were refined with the known $\mathrm{TbRe_2Al_{10}}$-type structure with Z=8 f.u. per cell;[11] the structure for R=Y and Ho–Lu were refined with the known $\mathrm{LuRe_2Al_{10}}$-structure type, with Z=12 (Ref. 12) (Table I). Within the $R\mathrm{Re_2Al_{10}}$ series, this is the first *Cmcm* structure report of $\mathrm{YRe_2Al_{10}}$ and $\mathrm{DyRe_2Al_{10}}$. The contraction of the structure with substitution of a smaller R is clearly seen from the unit cell volumes (Table I). Single crystal x-ray diffraction measurements established the stoichiometries of samples (Table II). For each $R\mathrm{Re_2Al_{10}}$ member, the deviation from the ideal composition was determined by individual refinement of the atomic occupancy parameter together with the anisotropic displacement parameter. For all compounds and within 3σ, rhenium sites did not deviate from full occupancies. For compounds with slightly deficient rare-earth sites (R=Gd, Tb, Dy, Tm, and Yb), mix occupancies with Al were not assumed, in spite of the fact that crystals formed in aluminum flux. Although this is an acceptable means of crystal composition refinement, there is evidence of aluminum site vacancies in crystals with R=Er and Lu. While the refined compositions are slightly off of stoichiometric R:Re:Al=1:2:10 amounts ($R\neq$ Y and Ho), for simplicity, they will continue to be noted as $R\mathrm{Re_2Al_{10}}$ in this report. As noted above, the refined cell volumes show smooth decrease expected from the lanthanoid contractions, with the anomaly that V/Z for $\mathrm{YbRe_2Al_{10}}$ is close to V/Z for $\mathrm{HoRe_2Al_{10}}$.

B. Physical properties

1. $\mathrm{YRe_2Al_{10}}$ and $\mathrm{LuRe_2Al_{10}}$

For $\mathrm{YRe_2Al_{10}}$, the magnetization signals at H=20 kOe are, to a first approximation, Pauli paramagnetic and slightly anisotropic with $M_\perp > M_\parallel$ at room temperature [Fig. 2(a)]. Below 50 K, there is an upturn that might indicate low concentration of paramagnetic impurities, also evident in the nonlinear behavior of the field-dependent magnetization at low fields and (<10 kOe) at 1.8 K (data not shown). For $\mathrm{LuRe_2Al_{10}}$ the magnetization at 20 kOe is temperature independent and slightly anisotropic with $M_{\parallel c} > M_{\perp c}$ [Fig. 2(a), inset]; the field-dependent magnetization at 1.8 K is linear (not shown). The specific heat data increase monotonically with increasing temperature [Fig. 2(b)]. For $\mathrm{YRe_2Al_{10}}$, by extrapolating a linear region found in C/T versus T^2 between ~2 and 7 K (inset), a Debye temperature of $\theta_\mathrm{D}\approx 450$ K and an electronic contribution of $\gamma=16(1)$ mJ mol^{-1} K^{-2} [1.2(1) mJ mol^{-1} atom^{-1} K^{-2}] are found. For $\mathrm{LuRe_2Al_{10}}$, the electronic contribution is estimated at $\gamma=11(1)$ mJ mol^{-1} K^{-2} [0.83(5) mJ/mol atom K^2] and $\theta_\mathrm{D}\approx 460$ K. The temperature-dependent resistivity data

TABLE II. Atomic occupancy refinements for $R\mathrm{Re_2Al_{10}}$ *Cmcm* series

		Occupation ≠ 1		
	Wyckoff	$\mathrm{Gd_{0.966(3)}Re_2Al_{10}}$	$\mathrm{Tb_{0.981(2)}Re_2Al_{10}}$	$\mathrm{Dy_{0.973(4)}Re_2Al_{10}}$
R(1)	4*c*	0.933(5)	0.962(4)	0.946(7)
R(2)	4*a*			

		$\mathrm{YRe_2Al_{10}}$	$\mathrm{HoRe_2Al_{10}}$	$\mathrm{ErRe_2Al_{9.88(2)}}$	$\mathrm{Tm_{0.985(3)}Re_2Al_{10}}$	$\mathrm{Yb_{0.964(3)}Re_2Al_{10}}$	$\mathrm{LuRe_2Al_{9.6(1)}}$
R(1)	8*f*				0.977(4)	0.946(5)	
R(2)	4*c*						

[Fig. 2(c)] are consistent with a metal, manifesting a RRR ~ 9 ($\rho_{1.8\ \mathrm{K}} \approx 14\ \mu\Omega$ cm) for $\mathrm{YRe_2Al_{10}}$ and ~5.4 ($\rho_{1.8} \approx 25\ \mu\Omega$ cm) for $\mathrm{LuRe_2Al_{10}}$.

2. $\mathrm{GdRe_2Al_{10}}$

The temperature dependence of magnetization, in 100 Oe, is shown in Fig. 3(a). The $M(T)$ results along both crystallographic directions of $M_{\perp c}$ and $M_{\parallel c}$ separate into zfc and fc branches. At low temperatures and fields, $M_{\perp c} > M_{\parallel c}$. The magnetization increases below ~8 K with irreversibility in zfc/fc temperatures below ~7 K. The magnetization data, measured in an applied field of 5 kOe is plotted as H/M in the inset. The $M(T)$ results are essentially isotropic in the paramagnetic state. The Curie-Weiss temperatures and paramagnetic moments are summarized in Table III. For $\mathrm{GdRe_2Al_{10}}$, the derived μ_{eff} values are close to that expected for Gd^{3+} free ion ($7.94\mu_B$). Field-dependent magnetization data at 1.8 K are shown in Fig. 3(b); and the expected $7\mu_B/Gd^{3+}$ is approximately reached. For one of $M_{\perp}$ directions, a coercive field of $B_c \approx 2.25$ kOe and remanent magnetization of $M_r \approx 0.17\mu_B$ f.u.$^{-1}$ [Fig. 3(b), inset] are found. The noted hystereses in low-field zfc/fc temperature-dependent magnetization and the field-dependent magnetization at 1.8 K indicate that there is a small ferromagnetic component to the ordered state in $\mathrm{GdRe_2Al_{10}}$, despite the small negative θ_p of 5.6(1) K (Table II). In order to locate the magnetic transition temperature for $\mathrm{GdRe_2Al_{10}}$, magnetization isotherms in the vicinity of Curie temperatures have been measured for $M_{\perp c}$ and used for the construction of Arrott plots in the form of M^2 versus $H_{\mathrm{eff}}M^{-1}$ [Fig. 3(c)]. According to this plot, 7.5 K $< T_c <$ 7.6 K. However, since

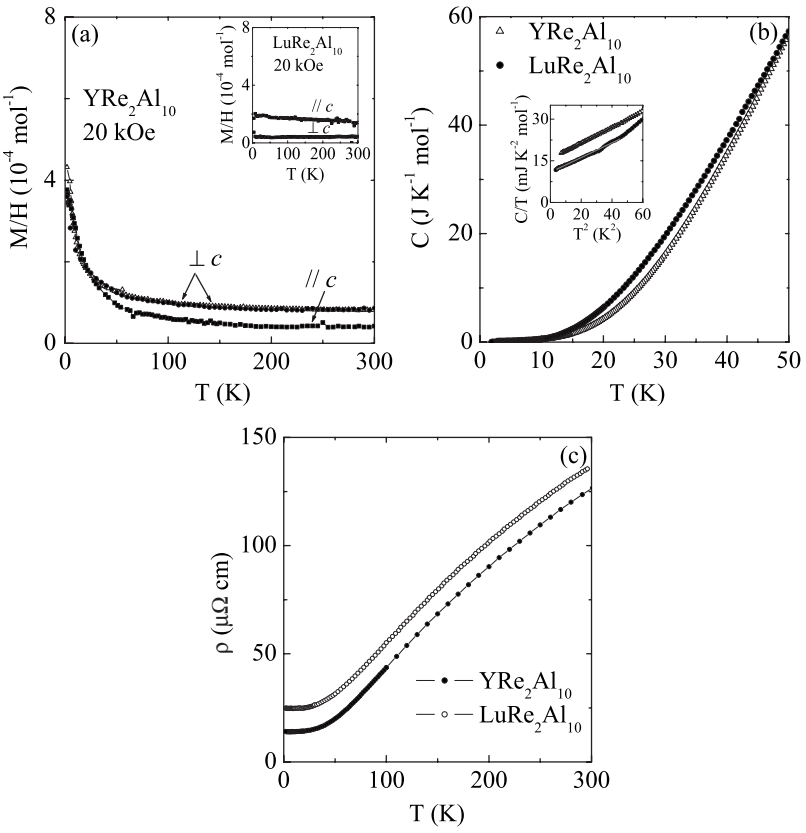

FIG. 2. For $\mathrm{YRe_2Al_{10}}$ and $\mathrm{LuRe_2Al_{10}}$, temperature dependence of (a) magnetization, (b) specific heat, and (c) electrical resistivity. Inset in (a) is the magnetization $\mathrm{LuRe_2Al_{10}}$. Inset in (b) is C/T versus T^2 dependence and linear fit of data in the range of 1.8– ~ 7 K.

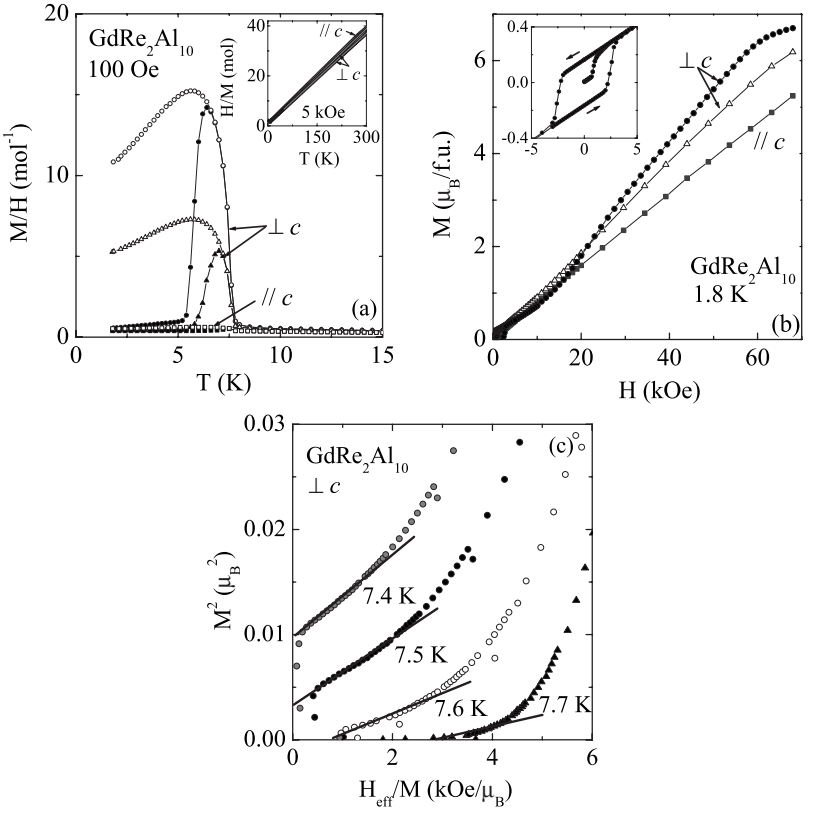

FIG. 3. For $GdRe_2Al_{10}$: (a) temperature dependence of magnetization in zero-field and field-cooled forms at 100 Oe; (b) field dependence of magnetization at 1.8 K; (c) Arrott plot of M^2 versus $H_{\mathrm{eff}}M^{-1}$ for $H \perp c$. Inset in (a) is the inverse of zero-field-cooled magnetization at 5 kOe, with Curie-Weiss fit above 50 K. Inset in (b) is the behavior in low-field regions for one of $H \perp c$.

the transition in $GdRe_2Al_{10}$ may not be purely ferromagnetic, the use of Arrott analysis is uncertain.

The transition to long-range magnetic order can be seen in zero-field specific heat results, displayed in Fig. 4(a), with anomaly at 7.2(1) K. For $GdRe_2Al_{10}$, this data accurately represent its ordering temperature. The magnetic specific heat results (C_m) are depicted in the inset, along with magnetic entropy, S/R. The eightfold ground states [for $Gd^{3+}J=7/2$, $R \ln 8 \approx 2.08R$] are recovered. The temperature-dependent electrical resistivity data are shown in Fig. 4(b). The RRR for $GdRe_2Al_{10}$ is 4 ($\rho_{1.8\ \mathrm{K}} \approx 31\ \mu\Omega$ cm). The ρ manifests a drop below ~7.5 K (inset), consistent with a decrease in magnetic scattering in the ordered state.

3. $TbRe_2Al_{10}$

The magnetization as a function of temperature for $TbRe_2Al_{10}$, at 100 Oe applied field, is anisotropic at low temperatures [Fig. 5(a)]. Along two crystallographic directions, magnetic ordering is clearly visible at 5.5 K, with a second magnetic feature below 3 K, noted by the divergence of zfc and fc results. This ferromagnetic feature may be due to an impure phase, or short-range ordering. The magnetization data, measured in an applied field of 10 kOe is plotted as H/M in the inset. The inverse of the polycrystalline temperature-dependent magnetization gives an effective moment of $9.7\mu_B$, comparable to the expected free Tb^{3+}. The Curie-Weiss temperature is −7.3(1)K, consistent with antiferromagnetic exchange interactions (Table III). Metamagnetism and slight anisotropy are evident in the 1.8 K field-dependent magnetization [Fig. 5(b)]. At the highest measured field of 68 kOe for $M_{\|c}$, the magnetization does not reach the expected saturated moment of $9\mu_B/Tb^{3+}$, may be due to crystal-field anisotropy or further, higher magnetic field metamagnetic transitions.

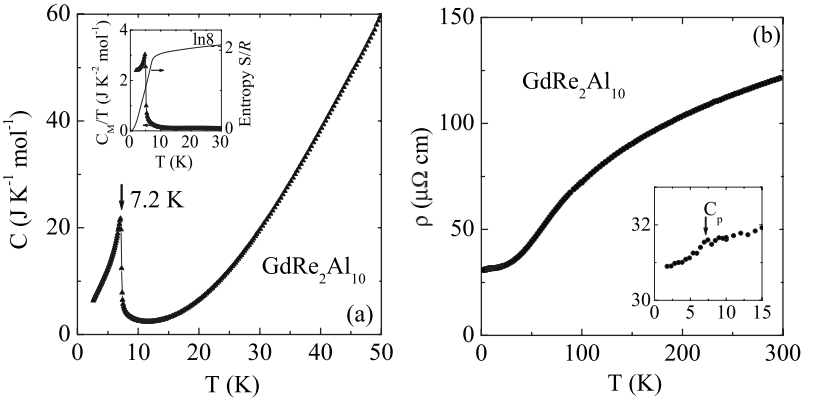

FIG. 4. For $GdRe_2Al_{10}$, temperature dependence of (a) specific heat and (b) resistivity. The inset in (a) is the magnetic specific heat in the form of C_M/T and also entropy change (S). The inset in (b) is the enlarged low-temperature region, with location of specific heat anomaly marked as C_p.

TABLE III. For $R\mathrm{Re}_2\mathrm{Al}_{10}$, paramagnetic effective moment (μ_{eff}), paramagnetic Curie-Weiss temperature (θ_{p}), and temperature independent term (χ_{o}). The moment (μ) found at 1.8 K and at ~60 kOe is also listed. The χ_{poly} represents the polycrystalline averaged magnetization data (see text).

	μ_{eff} (μ_{B})	θ_{p} (K)	μ (μ_{B})	χ_{o} (emu/mol)
		$GdRe_2Al_{10}$		
$\parallel c$	7.8	−6.9(4)	5.2	0.0007(1)
$\perp c$	7.9	−5.5(2)	6.5	0.00004(2)
$\perp c$	8.0	−5.6(1)	6.2	0.00038(2)
χ_{poly}	7.9	−5.6(1)		0.00014(2)
		$TbRe_2Al_{10}$		
$\parallel c$	9.4	6.2(2)	5.7	0.0006(1)
$\perp c$	10.4	−29.8(3)	4.0	−0.0025(1)
$\perp c$	9.4	−2.2(2)	4.5	0.0009(1)
χ_{poly}	9.7	−7.3(1)		−0.00019(4)
		$DyRe_2Al_{10}$		
$\parallel c$	10.4	−12.4(5)	6.6	0.0017(2)
$\perp c$	10.2	5.5(3)	6.6	0.0009(1)
$\perp c$	10.5	−5.9(4)	6.3	−0.0007(2)
χ_{poly}	10.3	−3.1(2)		0.0012(1)
		$HoRe_2Al_{10}$		
$\parallel c$	10.8	−2.7(2)	7.3	−0.0001(1)
$\perp c$	10.9	−12.1(2)	5.2	−0.0018(1)
$\perp c$	10.5	−2.6(2)	6.2	0.0001(1)
χ_{poly}	10.7	−3.8(1)		−0.00052(4)
		$ErRe_2Al_{10}$		
$\parallel c$	9.5	−7.5(1)	6.1	−0.00034(3)
$\perp c$	9.7	−0.3(3)	4.7	−0.0004(1)
$\perp c$	9.4	−2.6(1)	4.2	0.00009(5)
χ_{poly}	9.5	−3.5(1)		−0.00019(2)
		$TmRe_2Al_{10}$		
$\parallel c$	7.2	−22.8(7)	3.4	0.0011(1)
$\perp c$	7.8	10.8(3)	4.4	−0.0015(1)
$\perp c$	8.0	−16.4(4)	2.9	−0.0014(1)
χ_{poly}	7.6	−9.0(2)		−0.00013(3)
		$YbRe_2Al_{10}$		
$\parallel c$	4.4	−128(3)		0.0013(1)
$\perp c$	4.9	−161(4)		0.0002(1)
χ_{poly}	4.7	−151(3)		0.0006(1)

The specific heat data show a transition at 5.0(3) K [Fig. 6(a)]. The estimated magnetic contribution to specific heat is shown in the inset, alongside entropy. The total entropy below T_{N} is found to be ~80% R ln 2, and much less than the expected value of $2.56R(J=6)$. This signifies contribution from crystal-field effects. Tb, a non-Kramer ion, may have a singlet ground state, with the first excited level within $\sim T_{\mathrm{N}}$ so as to allow for magnetic order in $TbRe_2Al_{10}$ at $T_{\mathrm{N}}=5.0(3)$K. The electrical resistivity decreases with lowering temperature and shows a clear drop below ~5 K, due to the loss of spin disorder scattering in the antiferromagnetic ordered state [Fig. 6(b)]. The $\rho(T)$ data manifest a RRR of only 3.2 and $\rho_{1.8\ \mathrm{K}} \approx 110\ \mu\Omega$ cm. The feature in $\rho(T)$ coincides with the position of averaged polycrystalline $d(\chi T)/dT$ peak and $C(T)$ anomaly [Fig. 6(c)].

4. $DyRe_2Al_{10}$

The magnetization as a function of temperature at 100 Oe from $DyRe_2Al_{10}$ is nearly isotropic with $M_{\parallel c} \sim M_{\perp c}$ [Fig. 7(a), top inset]. There is no magnetic feature down to 1.8 K, with overlapping zfc/fc results. The inverse of the temperature-dependent magnetization (Fig. 7(a), Table III) gives a polycrystalline effective moment of $10.3\mu_{\mathrm{B}}$, close to the free ion $\mu_{\mathrm{eff}}=10.65\mu_{\mathrm{B}}$ value for Dy^{3+}; $\theta_{\mathrm{p}}=-3.1(2)$K. Field-dependent magnetization isotherms at 1.8 K (shown in inset) rapidly rise up to ~10 kOe, and continue to rise more gradually, with $M_{\parallel c} > M_{\perp c}$. No metamagnetic states are evident and the moment at ~60 kOe is not the full gJ value of the free $10\mu_{\mathrm{B}}$/Dy.

The specific-heat measurement gives a broad feature between 12 and 5 K, probably associated with a crystal electric field (CEF) splitting of Hund's ground-state multiplet [Fig. 7(b)]. The specific heat rises sharply below 3 K and results in a lambda anomaly at 1.7 K. Without $T<1.8$ K magnetization data, it is not possible to distinguish between ferromagnetic or antiferromagnetic ordering. For $DyRe_2Al_{10}$, magnetic entropy rapidly increases up to the magnetic transition temperature (inset). The magnetic entropy change up to T_{mag} is approximately R ln 2, indicating a doublet ground state. The entropy at 30 K is $1.5R$, small compared to the expected R ln 16 value (=2.77 R) for Dy^{3+}, indicating the presence of strong crystalline electric field splitting. The electrical resistivity [Fig. 7(c)] decreases with decreasing temperature down to 1.8 K, with RRR of ~5.6 and $\rho_{1.8\ \mathrm{K}} \approx 30\ \mu\Omega$ cm.

5. $HoRe_2Al_{10}$

The temperature-dependent magnetization data on $HoRe_2Al_{10}$ show no ordering down to 1.8 K [Fig. 8(a), top inset]. The high-temperature magnetization data follow the Curie-Weiss [Fig. 8(a)] and from the polycrystalline average $\mu_{\mathrm{eff}}=10.7\mu_{\mathrm{B}}$ (Ho^{3+}: $10.6\ \mu_{\mathrm{B}}$ theory) and $\theta_{\mathrm{p}}=-3.8(1)$ K (Table III). The field-dependent magnetization measurement is shown in Fig. 8(a), bottom inset. The $M_{\parallel c}$, has relatively a steeper rise at low fields and gives $7.3\mu_{\mathrm{B}}$ under 65 kOe, smaller than the expected saturation value of $10\mu_{\mathrm{B}}$.

The specific heat data show a broad feature between 6 and 1 K, probably associated with crystal electric field contribution, and a steep rise below 1 K [Fig. 8(b)]. $HoRe_2Al_{10}$ probably has an ordering temperature at or slightly below 0.4 K. The electrical resistivity [Fig. 8(b), inset] decreases with decreasing temperature with RRR of ~3.4 and $\rho_{1.8\ \mathrm{K}} \approx 86\ \mu\Omega$ cm.

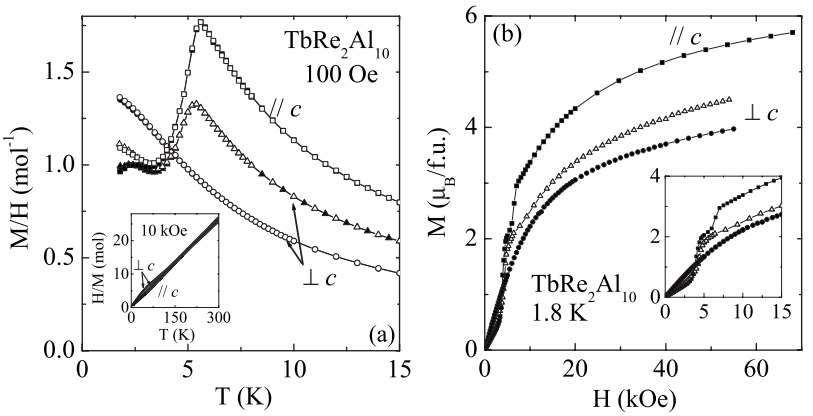

FIG. 5. For $TbRe_2Al_{10}$: (a) temperature dependence of magnetization in zero-field and field-cooled forms at 100 Oe; (b) field dependence of magnetization at 1.8 K. Inset in (a) is the inverse of zero-field-cooled magnetization at 10 kOe, with Curie-Weiss fit above 50 K. Inset in (b) is the behavior in low-field regions.

6. $ErRe_2Al_{10}$

The magnetization as a function of temperature at 100 Oe for $ErRe_2Al_{10}$ is paramagnetic down to 1.8 K [Fig. 9(a), top inset], with overlapping zfc/fc data and $M_{\|c} > M_{\perp c}$. The magnetization measurements at 10 kOe are nearly isotropic [Fig. 9(a)] and the Curie-Weiss fit to the high temperature, polycrystalline results yield values of $\mu_{\mathrm{eff}}=9.5\mu_B$ (Er^{3+}:$9.58\mu_B$ theory) and $\theta_p=-3.5(1)$ K. The magnetization does not reach saturation at 68 kOe (bottom inset).

The specific heat result has a feature probably due to CEF between 10 and 3 K, followed by an anomaly at $T_{\mathrm{mag}}=1.1(2)$ K [Fig. 9(b)], most likely associated with magnetic order. The magnetic entropy change up to T_{mag} is approximately $R \ln 2$, indicative of a doublet ground state or two closely spaced singlets. The continuous increase in S above T_M indicates that the electronic levels this compound is CEF split with closely spaced sublevels (top inset). The temperature dependence of electrical resistivity gives a RRR of 3.6, and $\rho_{1.8\ \mathrm{K}} \approx 49\ \mu\Omega$ cm (bottom inset).

7. $TmRe_2Al_{10}$

The magnetization as a function of temperature at 1 kOe for $TmRe_2Al_{10}$ has $M_{\|c} < M_{\perp c}$ [Fig. 10(a), top inset] with the overlap of the zfc/fc data down to 1.8 K and shows no sign of long-range magnetic order. The inverse of the temperature-dependent polycrystalline magnetic susceptibility follows the Curie-Weiss above 50 K [Fig. 10(a), Table III] and yields a polycrystalline effective moment of $7.6\mu_B$/Tm and an averaged $\theta_p=-9.0(2)$ K. The calculated effective moment is close to that expected for $Tm^{3+}(7.57\mu_B)$. Field dependent magnetization isotherms at 1.8 K are shown in Fig. 10(a), bottom inset. The moment at ~60 kOe is not the full gJ value of the free $7\mu_B$/Tm.

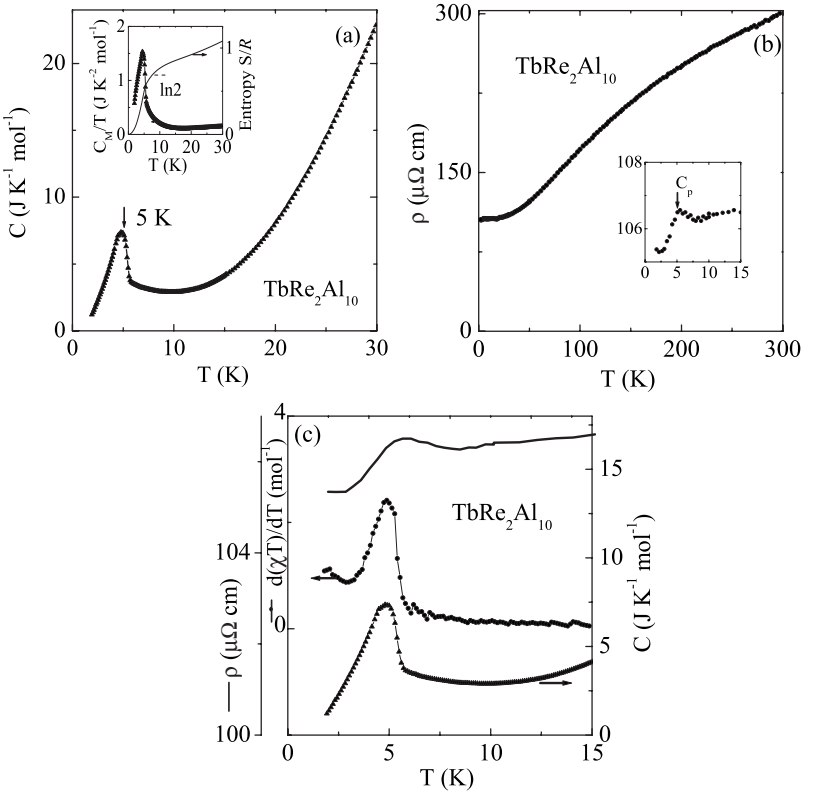

FIG. 6. For $TbRe_2Al_{10}$, temperature dependence of (a) specific heat and (b) electrical resistivity. Inset in (a) is the temperature dependence of magnetic specific heat and entropy change (s) for $TbRe_2Al_{10}$. Inset in (b) is the enlarged low-temperature $\rho(T)$ region, with location of specific heat anomaly marked as C_p. (c) For $TbRe_2Al_{10}$, the average susceptibility form $d(\chi T)/dT$ (H =100 Oe), also $\rho(T)$ and $C(t)$ data overlapped below 15 K.

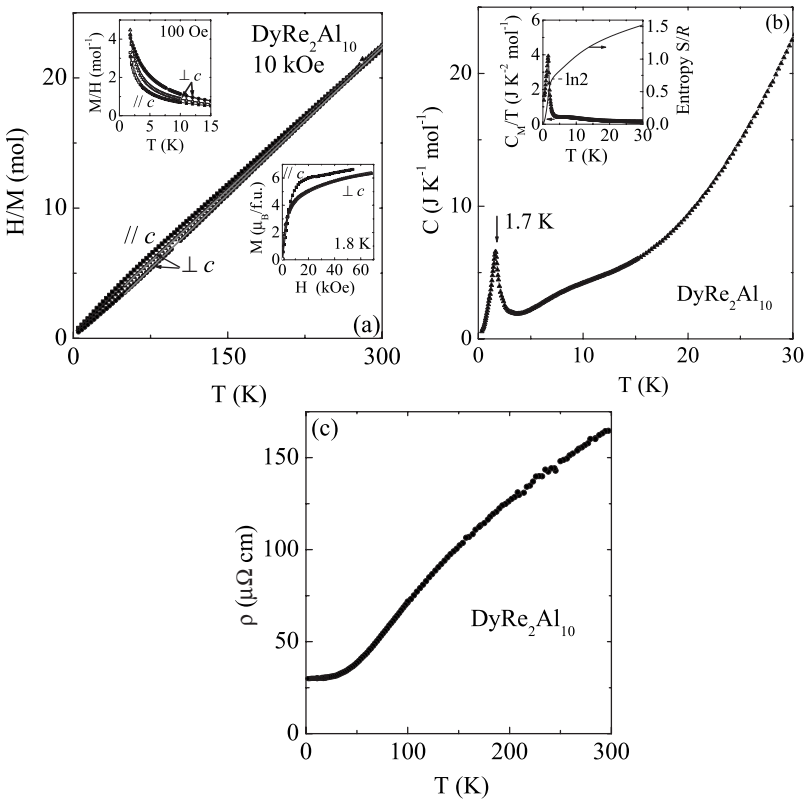

FIG. 7. For $DyRe_2Al_{10}$, (a) the inverse of zero-field-cooled magnetization at 10 kOe with Curie-Weiss fit above 50 K, temperature dependence of (b) specific heat and (c) resistivity. In (a), the top inset is the temperature dependence of magnetization in zero-field and field-cooled forms at 100 Oe and bottom inset is the field dependence of magnetization at 1.8 K. Inset in (b) is the temperature dependence of magnetic specific heat and entropy change (s).

The specific heat results are shown in Fig. 10(b). There is a broad anomaly in region of 12–3 K, and a second developing below 2.5 K. For $TmRe_2Al_{10}$ there is probably no magnetic ordering. The temperature dependence of electrical resistivity [Fig. 10(b), inset] gives a RRR of 3.7, with $\rho_{1.8\ K} \approx 82\ \mu\Omega$ cm.

8. $YbRe_2Al_{10}$

The magnetization as a function of temperature at 1 kOe is shown in Fig. 11(a). The data are anisotropic below ~100 K, with $M_{\parallel c} > M_{\perp c}$. The zfc/fc data along each measured crystallographic direction overlap with approximately linear behavior in field-dependent magnetization (bottom inset). For $M_{\perp c}$ there is a broad maximum at ~60 K, which is likely due to Kondo/mixed valence. The inverse of magnetization data as a function of temperature is reminiscent of a Curie-Weiss law with a very large paramagnetic Curie temperature of −151(3) K (top inset), indicative of antiferromagnetic correlations perhaps corresponding to the energy scale of valence fluctuations. The derived polycrystalline effective magnetic moment of $4.7\mu_B$/f.u. is close to the value for a free Yb^{3+} ion ($\mu_{eff}=4.54\mu_B$).

$YbRe_2Al_{10}$ does not order magnetically down to 1.8 K [Fig. 11(b)], as indicated by specific heat results [Fig. 11(b)]. By extrapolating a linear region found in C/T versus T^2 between ~2 and 6 K (inset), a Debye temperature of $\theta_D \approx 405$ K and an electronic contribution of $\gamma = 94(1)$ mJ mol^{-1} K^{-2} [7.2(1) mJ/mol atom K^2] are found. The temperature dependence of electrical resistivity [Fig. 11(c)] gives a RRR of 3.1 ($\rho_{1.8\ K} \approx 42\ \mu\Omega$ cm), with no feature in resistivity around 60 K. The occurrence of a AT^2 term in the resistivity (inset), is suggestive of a low-temperature Fermi-liquid state. For fits below ~6 K, A coefficients is 0.0011(1) $\mu\Omega$ cm K^{-2}.

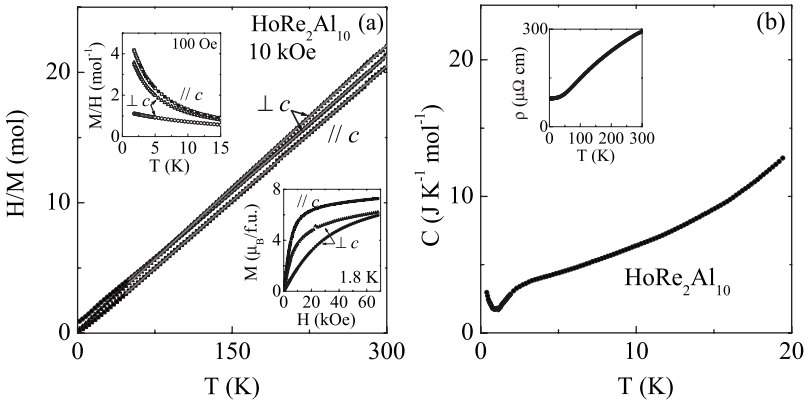

FIG. 8. For $HoRe_2Al_{10}$, (a) the inverse of zero-field-cooled magnetization at 10 kOe, with Curie-Weiss fit above 50 K, and (b) temperature dependence of specific heat. Insets of (a) are the temperature dependence of magnetization in zero-field and field-cooled forms at 100 Oe (top) and field dependence of magnetization at 1.8 K (bottom). Inset of (b) is the temperature dependence of electrical resistivity.

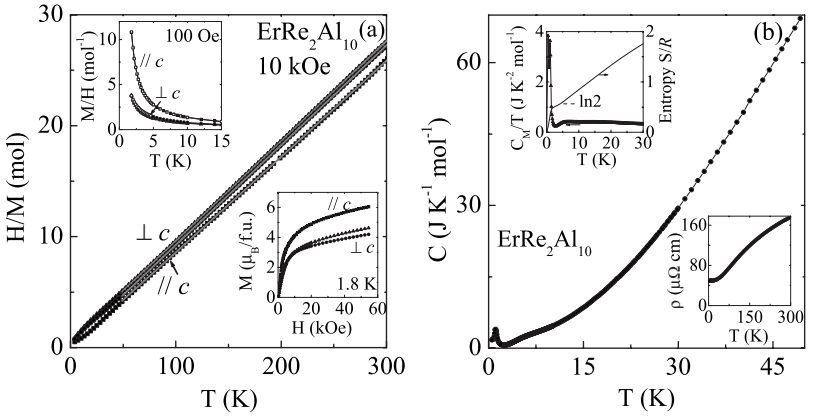

FIG. 9. For $ErRe_2Al_{10}$, temperature dependence of the (a) inverse of zero-field-cooled magnetization at 10 kOe, with Curie-Weiss fit above 50 K magnetization and (b) specific heat. Insets of (a) are the temperature dependence of magnetization in zero-field and field-cooled forms at 100 Oe (top) and the field dependence of magnetization at 1.8 K (bottom). Top inset of (b) is the temperature dependence of magnetic specific heat and entropy change (s); bottom inset of (b) is the dependence of resistivity.

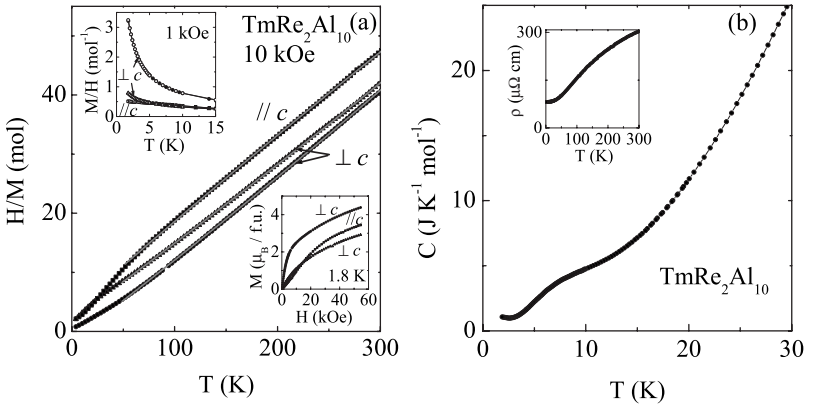

FIG. 10. For $TmRe_2Al_{10}$, temperature dependence of the (a) inverse of zero-field-cooled magnetization at 10 kOe, with Curie-Weiss fit above 50 K, and (b) specific heat. Insets of (a) are the temperature dependence of magnetization in zero-field and field-cooled forms at 1 kOe (top) and field dependence of magnetization at 1.8 K (bottom). Inset of (b) is the temperature dependence of electrical resistivity.

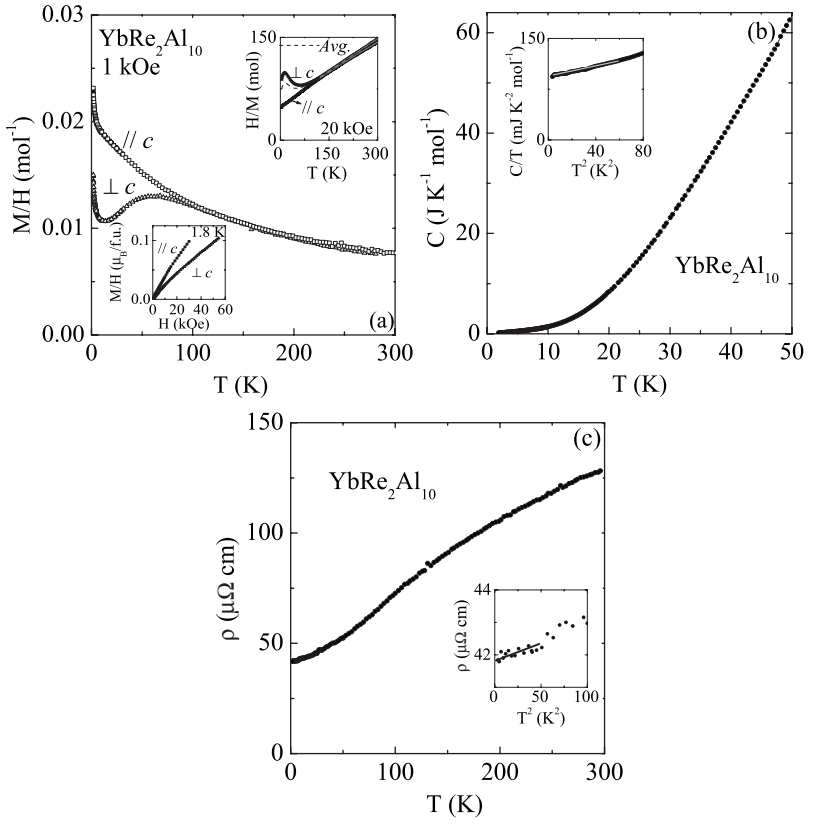

FIG. 11. For $YbRe_2Al_{10}$, temperature dependence of (a) magnetization at 1 kOe, (b) specific heat, and (c) resistivity. The bottom inset in (a) is the field dependence of magnetization at 1.8 K. Top inset in (a) is the inverse of temperature dependence of magnetization at 20 kOe above 5 K, along with the polycrystalline averaged data; Curie-Weiss fits are done above 125 K. The inset in (b) is the C/T versus T^2 dependence and linear fit of data in the range of 1.8 to 7 K. Inset of (c) is the linear fit in ρ versus T^2 between 1.8 and 6 K.

IV. CONCLUSIONS

The high-temperature magnetic behavior of all of the rhenium containing $R\mathrm{Re}_2\mathrm{Al}_{10}$ compounds, with the exception of the R=Y and Lu, is local momentlike and the effective moments calculated are essentially the free R^{3+} ion values for R=Gd-Yb. These μ_{eff} values along with θ_{p} constants are listed in Table III. The polycrystalline averaged Curie-Weiss temperatures are small and negative for R=Gd-Tm. This indicates that the coupling of the magnetic moments is weak. One effect that is characteristic of the indirect exchange interaction of R^{3+} ions by the Ruderman-Kittel-Kasuya-Yosida (RKKY) interaction is the scaling of quantities that are dependent on value of exchange interaction (θ_{p} and T_{M}) and de Gennes factor, $\mathrm{dG}=(g_J-1)^2J(J+1)$ (Ref. 20); here g_J is the Landé g factor and J is the total spin angular momentum. Although there is approximately constant values of paramagnetic Curie-Weiss temperature for the $R\mathrm{Re}_2\mathrm{Al}_{10}$ family the trend of magnetic ordering temperature versus dG is reasonable (Fig. 12). For $\mathrm{GdRe}_2\mathrm{Al}_{10}$ magnetic interaction between the Gd moments is the strongest of all members, as expected (J=7/2), with T_{c}=7.2(1) K. $\mathrm{TbRe}_2\mathrm{Al}_{10}$ orders antiferromagnetically at T_{N}=5.0(3) K. For R=Dy, Ho, and Er members, T_{mag}=1.7(1), $\leq$0.4, and 1.1(1) K, respectively. The non–de Gennes ordering among these latter members is probably associated with crystal-electric-field induced anisotropies. For R=Tm, the magnetic order is probably lost, evidenced by gradual upturn in specific heat below 3 K. $\mathrm{YbRe}_2\mathrm{Al}_{10}$ is found to be an example of a correlated electron system with an enhanced electronic specific heat of $\sim$95 mJ mol^{-1} K^2. If this is associated with a ground state doublet, then $\gamma T_{\mathrm{K}}\sim R\ln 2$ gives $T_{\mathrm{K}}\sim$60 K, a value that is consistent with the loss of local moment character in the lower temperature $\chi(T)$ data.

All $R\mathrm{Re}_2\mathrm{Al}_{10}$ compounds described here are metallic. The RRR values across the series ranges from $\sim$3 to 9. As a relation between RRR and the crystallographic quality of the sample is generally drawn, our values would suggest a fair crystal quality. Although some of $R\mathrm{Re}_2\mathrm{Al}_{10}$ are found to be slightly rare-earth deficient (R=Gd, Tb, Dy, Tm, and Yb) or aluminum deficient (R=Er and Lu), no correlation is seen between the values of RRR based on bulk resistivity measurements and site vacancies in crystals. Based on this, it appears that the slight crystallographic off-stoichiometries noted are not significant (Table II). On one hand, the moderate RRR values may imply small plane defects such as stacking faults or stoichiometric line defects, i.e., edge dislocations, which would increase the value of residual resistivity, lowering RRR. On the other hand, some of the scattering in $R\mathrm{Re}_2\mathrm{Al}_{10}$ compounds may have magnetic origin at low temperatures, as RRR in the nonmagnetic R=Y and Lu give highest values.

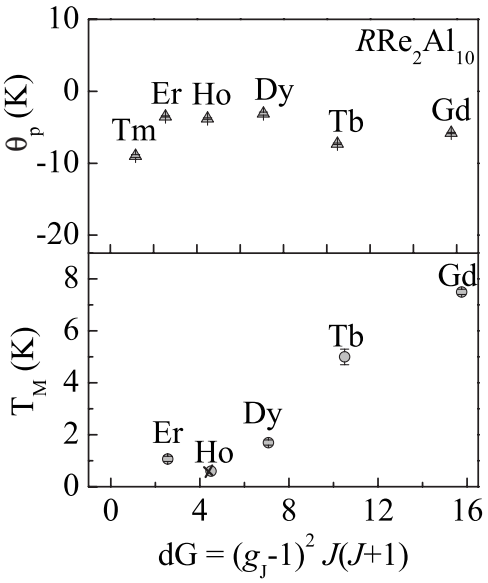

FIG. 12. For $R\mathrm{Re}_2\mathrm{Al}_{10}$ members, paramagnetic Curie-Weiss temperatures, θ_{P}, and magnetic ordering temperatures, T_{M}, as a function of de Gennes factor, dG.

ACKNOWLEDGMENTS

We are thankful to John D. Corbett for making single-crystal x-ray diffractometer available to us. Work at the Ames Laboratory was supported by the Department of Energy-Basic Energy Sciences under Contract No. DE-AC02-07CH11358.

[1] B. D. Rainford, C. J. Leavey, A. D. Hillier, and J. R. Stewart, Physica B **359-361**, 929 (2005).
[2] Y. Muro, S. Giri, G. Motoyama, H. Nakamura, and T. Kohara, J. Phys. Soc. Jpn. **74**, 1135 (2005).
[3] M. Coldea, M. Neumann, St. Lutkehoff, S. Mahl, and R. Coldea, J. Alloys Compd. **278**, 72 (1998).
[4] P. Schobinger-Papamantellos, P. Fischer, C. H. de Groot, F. R. de Boer, and K. H. J. Bushchow, J. Alloys Compd. **232**, 154 (1996).
[5] N. P. Duong, J. C. P. Klaasse, E. Bruck, I. H. Hagmusa, F. R. De Boer, and K. H. J. Buschow, J. Alloys Compd. **309**, L10 (2000).
[6] N. P. Duong, J. C. P. Klaasse, E. Bruck, F. R. De Boer, K. H. J. Buschow, J. Alloys Compd. **315**, 28 (2001).
[7] R. Nirmala, V. Sankaranarayanan, K. Sethupathi, T. Geethkumary, M. C. Valsakumar, Y. Hariharan, and A. V. Morozkin, Physica B **329-333**, 673 (2003).
[8] A. S. Sefat, B. Li, S. L. Bud'ko, and P. C. Canfield, Phys. Rev. B **76**, 174419 (2007).
[9] V. M. T. Thiede and W. Jeitschko, Z. Naturforsch., B: Chem. Sci. **53**, 673 (1998).
[10] G. Cordier, E. Czech, H. Ochmann, and H. Schaefer, J. Less-Common Met. **99**, 173 (1984).
[11] B. Fehrmann and W. Jeitschko, Z. Naturforsch., B: Chem. Sci. **54**, 1277 (1999).
[12] B. Fehrmann and W. Jeitschko, Inorg. Chem. **38**, 3344 (1999).
[13] IPDS II, Stoe and Cie Gmbh: Darmstadt, Germany, 2002.

[14] XSHAPE revision 2.03: Crystal Optimization for Numerical Absorbtion Correction; Stoe and Cie Gmbh:Darmstadt, Germany, 2003.
[15] SHELXTL, Bruker AXS, Inc.; Madison, WI, 2000.
[16] M. E. Fisher, Philos. Mag. **7**, 1731 (1962).
[17] P. Boutron, Phys. Rev. B **7**, 3226 (1973).
[18] B. D. Dunlap, J. Magn. Magn. Mater. **37**, 211 (1983).
[19] A. Arrott, Phys. Rev. **108**, 1394 (1957).
[20] P. G. De Gennes, J. Phys. Radium **23**, 510 (1962).